JUSAN SCIENCE

Journal of Engineering and Environmental Systems

ISSN (Print): 3135-2510; ISSN (Online): 3135-2529

journal homepage: https://jusanscience.com/journals/jees

Research Article

DFT Study of Glycidyl Methacrylate Copolymer Segments for Interactions with Copper and Lead Ions toward Wastewater Treatment Applications

Ainash Baidullayeva[1,2], Nesipkhan Bektenov[1,6], Anuar Aldongarov[3], Dana Kanzhigitova[4], Jia Li[5], and Mirat Karibayev[4*]

[1]Laboratory of Ion Exchange Resins and Membranes, A. B. Bekturov Institute of Chemical Sciences, Almaty 050010, Kazakhstan
[2]Department of Engineering Disciplines and Good Practices, School of Pharmacy, Asfendiyarov Kazakh National Medical University, Almaty 050010, Kazakhstan
[3]Department of Technical Physics, L. N. Gumilyov Eurasian National University, Astana 010000, Kazakhstan
[4]National Laboratory Astana, Nazarbayev University, Astana 010000, Kazakhstan
[5]School of Energy and Constructional Engineering, Shandong Huayu University of Technology, Dezhou 253034, Shandong, China
[6]Department of Chemistry, Abai Kazakh National Pedagogical University, Almaty 050010, Kazakhstan
**Corresponding author: Mirat Karibayev mirat.karibayev@nu.edu.kz*

https://doi.org/10.66973/jees.26.013

Article info:

Received: 08 October 2026 / Revised: 09 November 2026 / Accepted: 20 November 2026 / Published: 26 November 2026

Baidullayeva, A., Bektenov, N., Aldongarov, A., Kanzhigitova, D., Li, J., & Karibayev, M. (2026). DFT Study of Glycidyl Methacrylate Copolymer Segments for Interactions with Copper and Lead Ions toward Wastewater Treatment Applications. *Journal of Engineering and Environmental Systems*, 2, 184-196. https://doi.org/10.66973/jees.26.013

Abstract: This study uses density functional theory (DFT) to examine how a glycidyl methacrylate/acrylonitrile/polyethyleneimine (GMA/ACN/PEI) copolymer segment interacts with Cu(II) and Pb(II) in water. Geometry optimizations and frequency calculations were performed at the UB3LYP/LANL2DZ level using implicit solvation (IEFPCM) and a cluster-continuum model containing three explicit water molecules. Metal-ligand distances, quantum theory of atoms in molecules (QTAIM) descriptors, reduced density gradient/noncovalent interaction (RDG/NCI) maps, and electron localization functions were analyzed. Both metals coordinate primarily through oxygen atoms, whereas the tertiary amines act as hydrogen-bond and proton acceptors. Cu–O distances were 1.97–2.14 Å and exhibited predominantly closed-shell character. Pb binding involved hydroxyl proton transfer to a neighboring amine, directly or through a water bridge, generating a Pb-alkoxide contact (2.06–2.16 Å) with partial covalent character. Explicit water increased the coordination numbers and modified the hydrogen-bond networks. The distinct binding modes are consistent with the experimentally reported higher uptake of Pb(II) than Cu(II), although quantitative selectivity cannot be determined without aqueous complexation free energies.

© 2026 Jusan Science Publisher LTD. All rights reserved.
This is an open access article distributed under the terms of the Creative Commons Attribution (CC BY 4.0) license.

Keywords: *wastewater treatment; glycidyl methacrylate; acrylonitrile; polyethyleneimine; heavy metal ions; density functional theory; QTAIM; electron localization function.*

1 Introduction

Water contamination by heavy metal ions represents one of the most pressing environmental and public health challenges of the modern era. Copper and lead, in particular, are widely discharged into aquatic ecosystems through industrial activities such as mining, electroplating, battery manufacturing, and agricultural runoff. Metal ions can persist in aquatic environments, motivating research on ion-exchange, polymeric, and other adsorption-based treatment methods [1]–[7]. Broader concerns about drinking-water quality and co-occurring contaminants have also been reported [8]. Consequently, the development of efficient, cost-effective, and sustainable materials for heavy-metal removal has attracted considerable research attention [1], [3], [4]. Among wastewater treatment technologies, adsorption is attractive because of its operational simplicity, high removal efficiency, and potential cost-effectiveness [4], [5]. Advances in chelating resins, crosslinked hydrogels, functional polymer matrices, sensor-related polymer chemistry, and modified polymer adsorbents have demonstrated the versatility of tailored functional groups for environmental applications [3], [4], [9]–[17]. Glycidyl methacrylate (GMA)-based copolymers are particularly amenable to post-polymerization modification because their reactive epoxide groups can be functionalized with amines and other coordinating groups [1], [2], [9], [15]. Combining GMA with acrylonitrile (ACN) and polyethyleneimine (PEI) introduces nitrogen- and oxygen-containing donor sites that can participate in metal-ion retention [1], [2].

Recent experimental studies have demonstrated the effectiveness of modified GMA copolymers for the removal of copper, lead, chromium, and other metal ions from aqueous solutions [1], [2], [9], [14]. For instance, Bektenov et al. [1] reported that a GMA/ACN/PEI adsorbent removed both Cu(II) and Pb(II) ions, with a higher removal efficiency (85.6% vs 77.8%) and Langmuir capacity (15.25 vs 2.45 mg g^{-1}) for Pb(II) than for Cu(II), while El-Magied et al. [9] successfully utilized modified GMA resins for chromium(VI) removal. Despite these promising experimental findings, the molecular-level mechanisms governing metal ion binding to GMA copolymer segments remain insufficiently understood. A detailed understanding of the interaction between the polymer functional groups and metal ions is essential for the rational design of improved adsorbent materials with enhanced selectivity and capacity.

Density functional theory (DFT) provides molecular-level insight into coordination geometries and electronic interactions in polymer-metal systems [10], [16]. Computational studies can reveal noncovalent interactions that are difficult to characterize experimentally [10], [16]. Complementary work on functionalized resins, drinking-water quality, and polymeric adsorbents provides the experimental and environmental context for these applications [17]–[19]. However, a systematic DFT investigation of GMA/ACN/PEI copolymer segments interacting with copper and lead ions under different solvation conditions has not previously been reported.

In this work, we present a comprehensive DFT study of a GMA/ACN/PEI copolymer segment and its interactions with Cu(II) and Pb(II) ions in both implicit and explicit water environments. The objectives are to (i) elucidate the optimized geometries, coordination modes and electronic states of the copolymer-metal complexes, including quantitative metal-ligand distances; (ii) quantify the metal–ligand and hydrogen-bond interactions with QTAIM descriptors at the bond critical points and characterize them with RDG/NCI and ELF analyses; (iii) evaluate the influence of explicit water molecules on the binding modes; and (iv) compare the computed binding modes critically with the available experimental adsorption data for GMA/ACN/PEI adsorbents [1]. The findings are expected to provide a theoretical foundation for the design of GMA-based adsorbents for wastewater treatment applications.

❖

2 Materials and methods

All density functional theory (DFT) calculations were performed using Gaussian 16 software (Revision C.01) [20]. The molecular system investigated was a glycidyl methacrylate/acrylonitrile/polyethyleneimine (GMA/ACN/PEI) copolymer segment, selected as a representative model of the adsorbent material. The model segment ($C_{15}H_{29}N_3O_3$, 50 atoms; Figure 1) consists of one GMA repeat unit whose oxirane ring has been opened by a PEI-derived N,N,N′-trimethylethylenediamine fragment, giving a

© 2026 Jusan Science Publisher LTD. All rights reserved.
This is an open access article distributed under the terms of the Creative Commons Attribution (CC BY 4.0) license.

https://doi.org/10.66973/jees.26.013

secondary β-hydroxyl group adjacent to a tertiary amine, linked to an acrylonitrile-derived cyanoethyl unit; the backbone was truncated and saturated with methyl/hydrogen groups. This minimal unit contains all donor types present in the real adsorbent (ester carbonyl and ether oxygen atoms, a hydroxyl oxygen, two tertiary amine nitrogens and a nitrile nitrogen) while remaining tractable for wavefunction analysis; its limitations are discussed in Section 3.6. Five distinct systems were studied: (i) the pure GMA/ACN/PEI copolymer segment; (ii) the copolymer segment with a copper ion; (iii) the copolymer segment with a lead ion; (iv) the copolymer segment with a copper ion in the presence of explicit water molecules; and (v) the copolymer segment with a lead ion in the presence of explicit water molecules.

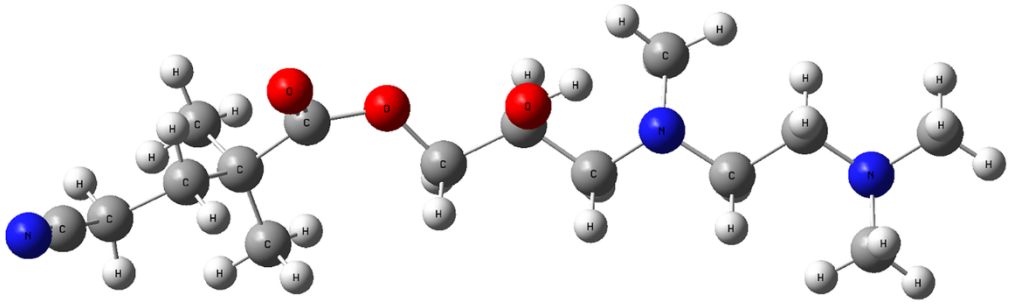

Figure 1. 3D chemical structure of GMA/ACN/PEI copolymer segment. Color key: gray, carbon; white, hydrogen; blue, nitrogen; red, oxygen.

Geometry optimizations and harmonic frequency calculations were carried out with the B3LYP hybrid functional [21], [22] in its spin-unrestricted form (UB3LYP) combined with the LANL2DZ basis set. For Cu and Pb, LANL2DZ uses the Hay–Wadt effective core potentials (ECPs) with double-ζ valence functions [23], [24], which also account implicitly for the scalar-relativistic effects that are essential for Pb; H, C, N and O are described by the all-electron D95V double-ζ basis. This level of theory was chosen because it is widely used for transition- and heavy-metal complexes of this size, treats both metals consistently and yields wavefunctions that can be analysed directly with Multiwfn; its known limitations (no polarization functions on light atoms, no dispersion correction and the delocalization error of hybrid functionals) are discussed in Section 3.6. The pristine copolymer segment was computed as a neutral closed-shell singlet (charge 0, multiplicity 1). All metal complexes were computed with a total charge of +2, corresponding to one divalent ion and a formally neutral ligand: the Cu(II) systems ($3d^9$) as doublets (multiplicity 2) and the Pb(II) systems ($6s^2$) as closed-shell singlets (multiplicity 1). The amine groups were modelled in their neutral form, representative of the near-neutral conditions under which amine-functionalized adsorbents bind divalent metals, and no constraints were imposed on proton positions, so that metal-induced proton transfer could occur during optimization. Bulk solvation was described with the IEFPCM model [25] using water as the solvent for all metal systems (implicit water). For systems (iv) and (v), three explicit water molecules were added around the metal ion and the resulting cluster was embedded in the same continuum (cluster-continuum model), so that specific metal-water and water-polymer hydrogen bonds could be described. Vibrational frequency calculations at the same level confirmed that all optimized structures are true minima on the potential energy surface (no imaginary frequencies).

The optimized geometries were visualized using GaussView 6 [26] and VMD [27]. Wavefunction analyses were conducted with Multiwfn [28]. Non-covalent interactions were analysed with the RDG function and its NCI representation [29], in which the sign of the second eigenvalue of the electron-density Hessian, $\mathrm{sign}(\lambda_2)\rho$, distinguishes attractive ($\mathrm{sign}(\lambda_2)\rho < 0$) from repulsive ($\mathrm{sign}(\lambda_2)\rho > 0$) contacts. Critical points of the electron density were located by QTAIM topology analysis [30], and the following descriptors were evaluated at each bond critical point (BCP): the electron density $\rho(r)$, its Laplacian $\nabla^2\rho(r)$, the Lagrangian kinetic (G), potential (V) and total ($H = G + V$) energy densities, the $|V|/G$ ratio, ELF and the spin density. Interactions were classified

© 2026 Jusan Science Publisher LTD. All rights reserved.
This is an open access article distributed under the terms of the Creative Commons Attribution (CC BY 4.0) license.

https://doi.org/10.66973/jees.26.013

following Espinosa et al. [31], [32]: $\nabla^2\rho > 0$ with $|V|/G < 1$ ($H > 0$) indicates a closed-shell (electrostatic) interaction; $\nabla^2\rho > 0$ with $1 < |V|/G < 2$ ($H < 0$) indicates an intermediate interaction with partial covalent character; and $|V|/G > 2$ indicates a shared (covalent) interaction. Local interaction energies were estimated as $E_{BCP} \approx \frac{1}{2}V(r_{BCP})$ [31]; because this relation was parameterized for hydrogen bonds, these values are used only as a relative indicator and not as binding energies. For the ECP-described metals, the core density was supplemented in the topology analysis with Multiwfn's built-in electron density functions (EDF). The ELF [33] was evaluated as two-dimensional maps and at the BCPs

3 Result and discussion

3.1 Coordination Modes, Electronic States, and Optimized Geometries.

Figure 2 presents the DFT-optimized geometries of the GMA/ACN/PEI copolymer segment in its pristine form and in complex with Cu and Pb under the two solvation models, and the key interatomic distances are collected in Table 1. In the pristine segment (Figure 2a), the β-hydroxyl group formed by epoxide ring opening donates an intramolecular hydrogen bond to the adjacent tertiary amine nitrogen (O–H···N = 1.946 Å), in agreement with the O–H···N(tertiary amine) hydrogen bond inferred from the FTIR spectra of the GMA/ACN/PEI adsorbent [1]. In implicit water, Cu (Figure 2b) is bound as a bidentate O,O-chelate by the ester carbonyl oxygen (Cu–O = 1.995 Å) and the hydroxyl oxygen (Cu–O = 1.965 Å; O–Cu–O = 114.6°); the hydroxyl proton is retained and its O–H···N hydrogen bond shortens to 1.871 Å. Coordination lengthens the C=O bond from 1.247 to 1.263 Å, as expected for σ-donation from the carbonyl oxygen to the metal. Pb (Figure 2c) adopts a different binding mode: the hydroxyl proton is transferred to the neighbouring tertiary amine (N–H = 1.040 Å; the remaining O···H–N^+ contact is 1.996 Å), and Pb binds the resulting alkoxide oxygen (Pb–O = 2.055 Å) together with the ester ether oxygen (2.417 Å) and, more weakly, the carbonyl oxygen (2.959 Å). None of the nitrogen atoms (tertiary amines or nitrile) coordinates either metal in any of the optimized structures; the shortest metal···N distances are 4.5–5.0 Å. The PEI amines therefore participate in metal binding indirectly, as hydrogen-bond and proton acceptors that stabilize the hydroxyl/alkoxide donor. The longer Pb–O than Cu–O distances reflect the larger ionic radius of Pb^{2+} (1.19 Å vs 0.73 Å for six-coordinate ions [34]).

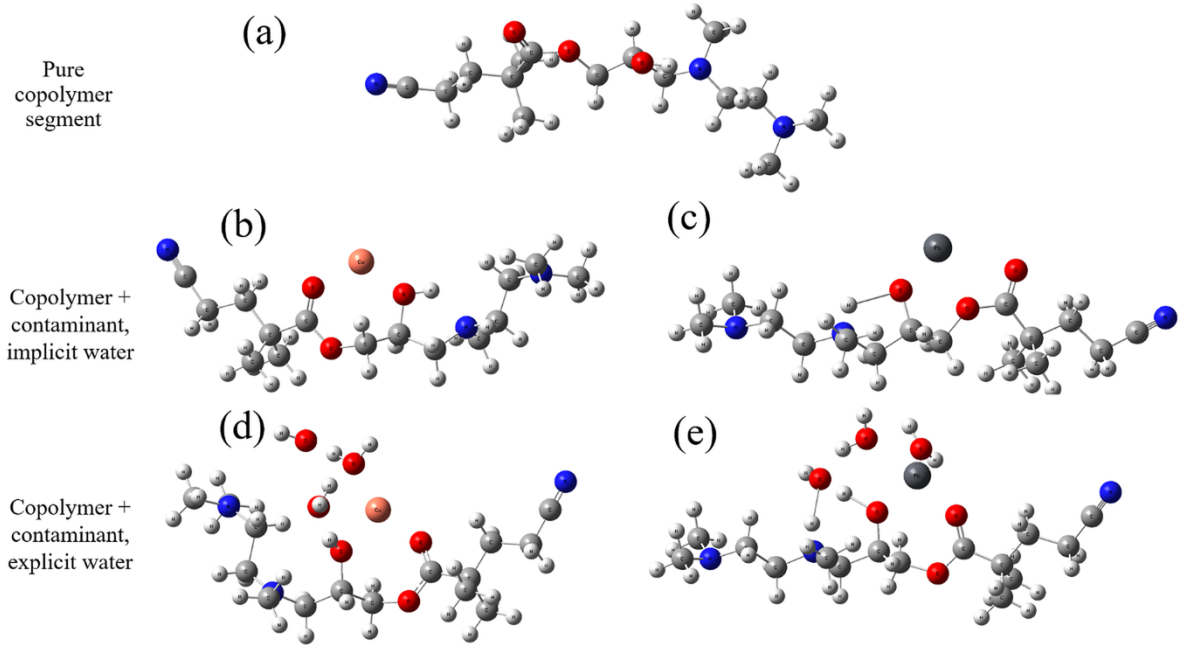

Figure 2. Optimized structures of (a) GMA/ACN/PEI copolymer segment, (b) GMA/ACN/PEI copolymer segment with copper ion (implicit water), (c) GMA/ACN/PEI copolymer segment with lead ion (implicit water), (d) GMA/ACN/PEI copolymer segment with copper ion in the presence of explicit water molecules, and (e) GMA/ACN/PEI copolymer segment with lead ion in the presence of explicit water molecules. Color key: gray, carbon; white, hydrogen; blue, nitrogen; red, oxygen; orange, copper; black, lead.

© 2026 Jusan Science Publisher LTD. All rights reserved.
This is an open access article distributed under the terms of the Creative Commons Attribution (CC BY 4.0) license.

https://doi.org/10.66973/jees.26.013

In the cluster–continuum models (Figures 2d and 2e), the explicit water molecules enter the coordination spheres of both metals. Cu (Figure 2d) is three-coordinate, bound to the carbonyl oxygen (1.995 Å), one water molecule (1.991 Å) and the hydroxyl oxygen (2.142 Å) in a T-shaped arrangement ($O_{C=O}$–Cu–O_w = 154.8°). The hydroxyl group is retained but now donates a short hydrogen bond to a second water molecule (1.577 Å), and the Cu-bound water is strongly polarized, donating a very short hydrogen bond (1.467 Å) to the third water molecule. For Pb (Figure 2e), the water molecules mediate a proton relay: the hydroxyl proton is transferred to a bridging water molecule (H–O_w = 1.050 Å; O···H = 1.460 Å), which in turn transfers one of its protons to the tertiary amine (N–H = 1.048 Å; N–H···O_w = 1.863 Å). Pb is bound to the alkoxide oxygen (2.163 Å), two water molecules (2.296 and 2.317 Å) and the carbonyl oxygen (2.558 Å). All four Pb–O bonds lie in one hemisphere (O38–Pb–O angles of 78.8–88.4°), i.e. a hemidirected geometry characteristic of a stereochemically active $6s^2$ lone pair of Pb(II) [35]. Explicit hydration thus increases the coordination number of both metals (Cu: 2 → 3; Pb: 3 → 4) without changing the binding modes identified in implicit water.

The electronic structure of the Cu systems requires comment. Although the complexes were computed as Cu(II) doublets, the spin density at all Cu–O BCPs is essentially zero ($|\rho_s| < 10^{-5}$ a.u.), whereas appreciable spin density is located on the PEI amine nitrogen atoms (0.20 a.u. at the N49 nuclear critical point in implicit water; 0.09 and 0.11 a.u. at N40 and N49 in explicit water). Consistently, these nitrogen atoms become planar (sum of C–N–C angles of 356.7–359.9° vs 336.0–339.6° in the pristine segment), their N–C bonds shorten (to 1.42–1.47 Å from 1.48 Å), and the CH_2–CH_2 bond linking the two amines is elongated (1.588 Å in implicit and 1.671 Å in explicit water; Table 1). These features indicate that, at the UB3LYP/LANL2DZ level, electron density is transferred from the tertiary amine to the metal, giving a reduced, Cu(I)-like centre and an aminium radical cation. Oxidation of amines by Cu(II) is chemically plausible, but hybrid functionals with 20% exact exchange are also known to over-stabilize such delocalized charge-transfer states [36]. This observation is therefore reported as a model sensitivity: the Cu results are interpreted in terms of Cu–O coordination geometry and bonding rather than as a definitive oxidation-state assignment (Section 3.6). The Pb systems are closed-shell and show no such ambiguity.

Table 1. Selected optimized interatomic distances (Å) and angles (°) at the UB3LYP/LANL2DZ level (M = Cu or Pb). $O_{C=O}$, carbonyl oxygen; O_{OH}/O_{alk}, hydroxyl/alkoxide oxygen; O_{est}, ester ether oxygen; O_w, water oxygen; N40/N49, tertiary amine nitrogens. Atom numbering follows that of the optimized structures.

Parameter	Copolymer	Cu, implicit	Pb, implicit	Cu, explicit	Pb, explicit
		Metal–ligand distances (Å)			
M–$O_{C=O}$ (O50)	–	1.995	2.959	1.995	2.558
M–O_{OH}/O_{alk} (O38)	–	1.965 (OH)	2.055 (alk)	2.142 (OH)	2.163 (alk)
M–O_{est} (O13)	–	3.337	2.417	3.550	> 4.0
M–O_w	–	–	–	1.991 (O55)	2.296 (O58); 2.317 (O55)
Shortest M···N	–	4.518 (N40)	4.681 (N40)	4.975 (N40)	4.733 (N40)
Coordination number (M–O ≤ 3.0 Å)	–	2	3	3	4
O–M–O angles (°)	–	114.6	71.1 (O38–Pb–O13)	97.0; 103.5; 154.8	78.8–88.4 (O38–Pb–O)
		Ligand geometry and proton position (Å)			
C12=O50	1.247	1.263	1.241	1.260	1.259
C23–O38	1.460	1.477	1.455	1.455	1.447
O38–H39	1.001	1.006	1.996	1.018	1.460
H39···N40 / N40–H	1.946 (O–H···N)	1.871 (O–H···N)	1.040 (N–H)	2.964	1.048 (N40–H53)
Water-mediated H-bonds	–	–	–	O38–H···O_w 1.577; O_w–H···O_w 1.467, 1.833	O38···H–O_w 1.460; N–H···O_w 1.863; O_w–H···O_w 1.577
ΣC–N–C at N40 / N49 (°)	339.6 / 336.0	343.2 / 359.9	335.7 / 337.9	359.7 / 356.7	333.9 / 337.9
C28–C31 (N–CH_2–CH_2–N)	1.543	1.588	1.542	1.671	1.542

© 2026 Jusan Science Publisher LTD. All rights reserved.
This is an open access article distributed under the terms of the Creative Commons Attribution (CC BY 4.0) license.

https://doi.org/10.66973/jees.26.013

3.2 Noncovalent Interactions: RDG and NCI Analysis

Figure 3 shows the RDG scatter plots (RDG versus sign(λ_2)ρ) and Figure 4 the corresponding NCI isosurfaces for the five systems. Because both representations derive from the same function, they are discussed together. Each low-RDG spike in Figure 3 corresponds to an isosurface in Figure 4, and its position on the sign(λ_2)ρ axis equals $-\rho$ at the associated BCP, so that the colour code (blue, strong attraction; green, van der Waals; red, steric repulsion) can be linked directly to the quantitative QTAIM values in Table 2. Because the scatter plots in Figure 3 are drawn for $-0.05 \leq \text{sign}(\lambda_2)\rho \leq 0.05$ a.u., the strongest metal–ligand features ($\rho_{BCP} > 0.05$ a.u.) fall outside the plotted window; they are identified from the blue isosurfaces in Figure 4 and quantified by the BCP values below.

In the pristine segment (Figures 3a and 4a), the only strongly attractive feature is the intramolecular O–H···N hydrogen bond (sign(λ_2)ρ = $-\rho_{BCP} \approx -0.036$ a.u.); the remaining isosurfaces are green van der Waals contacts between methyl/methylene groups (≈ -0.009 to -0.011 a.u.) and red ring-closure regions. On complexation in implicit water, new attractive features appear between the metal and its oxygen donors. For Cu (Figures 3b and 4b), they correspond to sign(λ_2)$\rho \approx -0.069$ to -0.076 a.u. (Cu–$O_{C=O}$ and Cu–O_{OH}), accompanied by the strengthened O–H···N hydrogen bond (-0.041 a.u.). For Pb (Figures 3c and 4c), the metal–ligand features span a wider range: a strongly attractive Pb–$O_{alkoxide}$ region (-0.111 a.u.), an intermediate Pb–O_{ester} contact (-0.049 a.u.) and a weak, largely green Pb···O=C contact (-0.017 a.u.). The more diffuse isosurfaces around Pb in Figure 4c therefore correspond to its longer secondary contacts and not to a weaker primary metal–ligand bond.

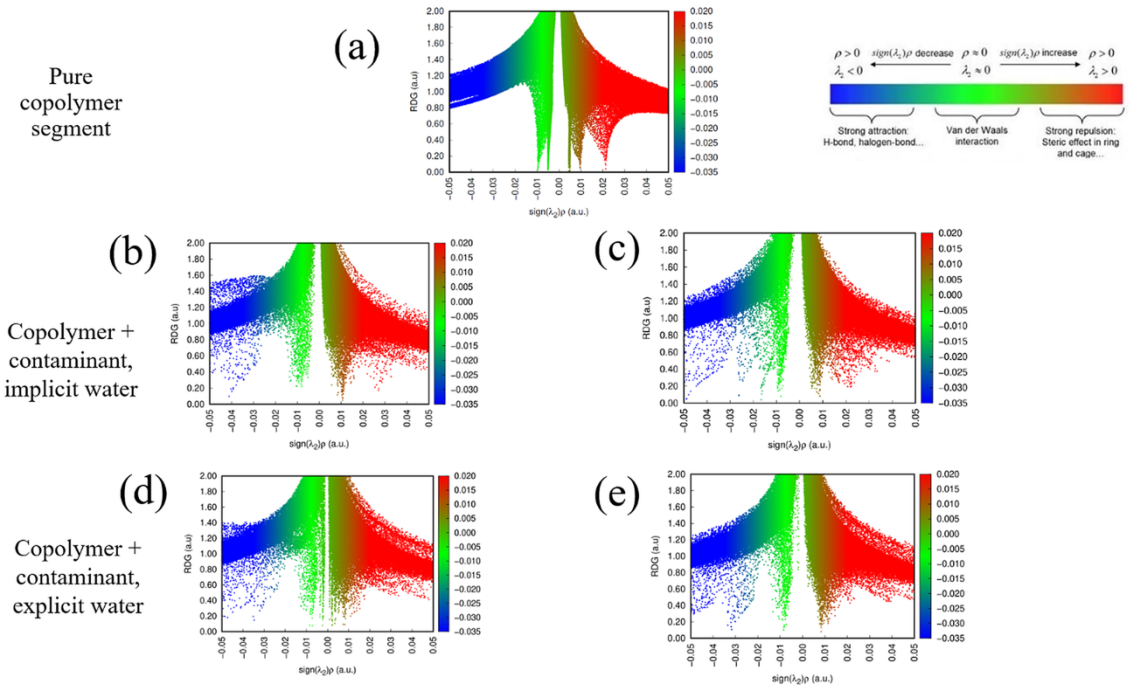

Figure 3. Reduced density gradients of (a) GMA/ACN/PEI copolymer segment, (b) GMA/ACN/PEI copolymer segment with copper ion (implicit water), (c) GMA/ACN/PEI copolymer segment with lead ion (implicit water), (d) GMA/ACN/PEI copolymer segment with copper ion in the presence of explicit water molecules, and (e) GMA/ACN/PEI copolymer segment with lead ion in the presence of explicit water molecules.

With explicit water (Figures 3d, 3e, 4d and 4e), additional blue–cyan regions appear for the water-mediated hydrogen bonds. In the Cu system, they correspond to the short hydrogen bond donated by the hydroxyl group to water (-0.063 a.u.) and to the hydrogen bond donated by the Cu-bound water (-0.079 a.u.), in addition to the three Cu–O contacts (-0.051 to -0.073 a.u.). In the Pb system, the strongest features are the Pb–$O_{alkoxide}$ bond (-0.087 a.u.) and the O···H–O_w proton-relay contact (-0.086 a.u.), followed by the two Pb–O_w bonds (-0.060 and -0.062 a.u.). Both metals are thus embedded in extended hydrogen-bond networks in which water acts simultaneously as a ligand and, for Pb, as a proton shuttle. Because the NCI analysis alone does not establish which metal is more strongly bound, the

© 2026 Jusan Science Publisher LTD. All rights reserved.
This is an open access article distributed under the terms of the Creative Commons Attribution (CC BY 4.0) license.

https://doi.org/10.66973/jees.26.013

interactions are quantified by QTAIM in the next section.

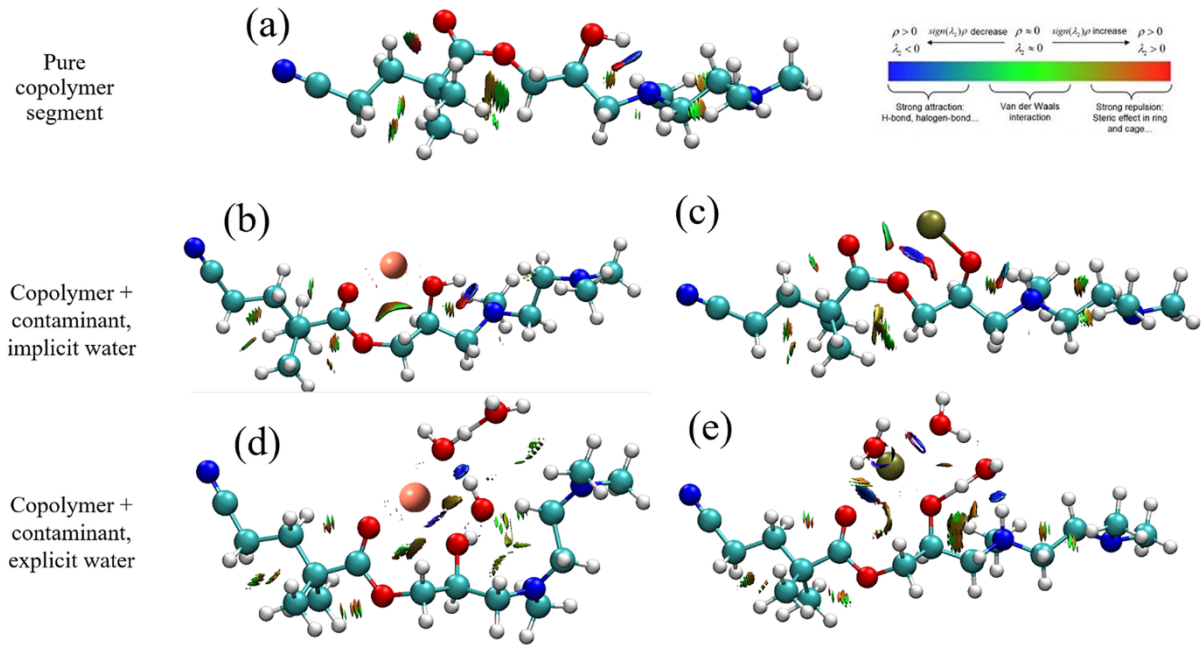

Figure 4. Non-covalent interactions of (a) GMA/ACN/PEI copolymer segment, (b) GMA/ACN/PEI copolymer segment with copper ion (implicit water), (c) GMA/ACN/PEI copolymer segment with lead ion (implicit water), (d) GMA/ACN/PEI copolymer segment with copper ion in the presence of explicit water molecules, and (e) GMA/ACN/PEI copolymer segment with lead ion in the presence of explicit water molecules. Color key: gray, carbon; white, hydrogen; blue, nitrogen; red, oxygen; light orange, copper; black orange, lead.

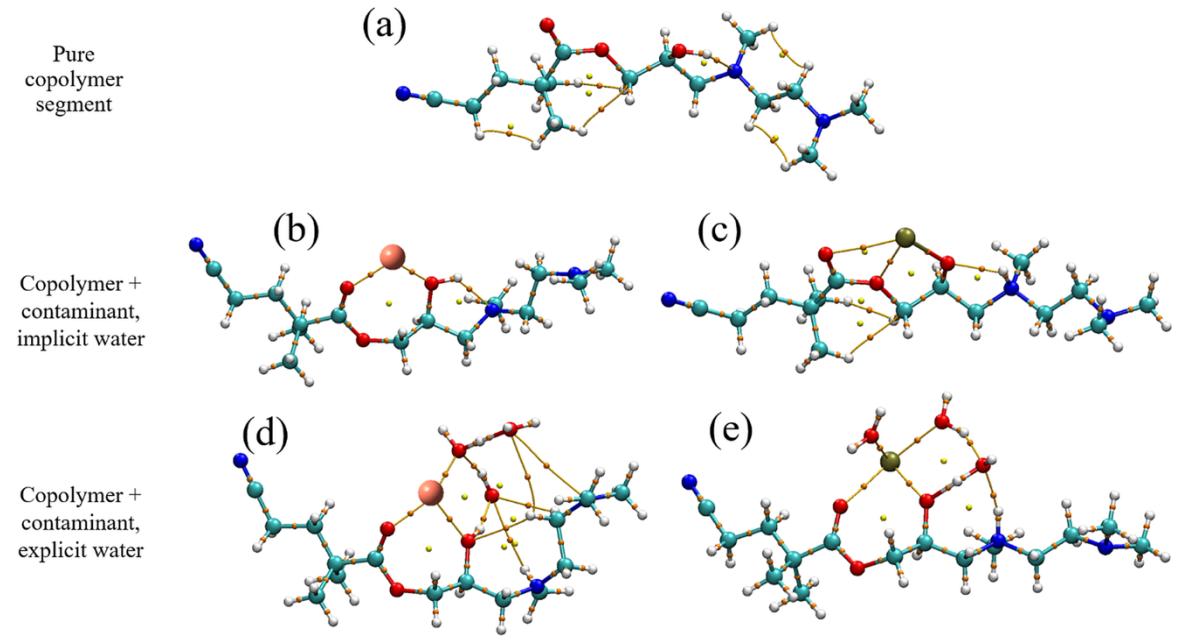

Figure 5. Critical points of (a) GMA/ACN/PEI copolymer segment, (b) GMA/ACN/PEI copolymer segment with copper ion (implicit water), (c) GMA/ACN/PEI copolymer segment with lead ion (implicit water), (d) GMA/ACN/PEI copolymer segment with copper ion in the presence of explicit water molecules, and (e)

© 2026 Jusan Science Publisher LTD. All rights reserved.
This is an open access article distributed under the terms of the Creative Commons Attribution (CC BY 4.0) license.

https://doi.org/10.66973/jees.26.013

GMA/ACN/PEI copolymer segment with lead ion in the presence of explicit water molecules. Color key: gray, carbon; white, hydrogen; blue, nitrogen; red, oxygen; light orange, copper; black orange, lead.

3.3 QTAIM Analysis of Metal–Ligand and Hydrogen-Bond Interactions.

Figure 5 shows the critical points located by QTAIM topology analysis. Besides the BCPs of the covalent framework, every metal–ligand and hydrogen-bond interaction discussed above is supported by a bond path and a BCP, and ring critical points appear inside the chelate rings formed by the metal, its donor atoms and the hydrogen-bonded groups. The descriptors of all metal–ligand and key hydrogen-bond BCPs are listed in Table 2.

For the pristine segment (Figure 5a), the O–H···N hydrogen bond has ρ = 0.036 a.u., $\nabla^2\rho$ = 0.101 a.u., a slightly negative H (−0.003 a.u.) and |V|/G = 1.11, i.e. a moderately strong hydrogen bond with partial covalent character (E_{BCP} ≈ −9.8 kcal mol^{-1}); the remaining non-covalent BCPs (C–H···H–C and C–H···C contacts) have ρ ≈ 0.009–0.011 a.u. and are purely closed-shell. The Cu–O BCPs in implicit water (Figure 5b) have ρ = 0.069–0.076 a.u., large positive Laplacians (0.53–0.58 a.u.), H ≈ 0 (−0.0004 to +0.0021 a.u.) and |V|/G = 0.98–1.00. They lie at the boundary between closed-shell and intermediate interactions and are dominated by the electrostatic component, as expected for a compact cation interacting with neutral oxygen donors; their large kinetic and potential energy densities reflect the short Cu–O distances. The Pb system (Figure 5c) shows a broader hierarchy: the Pb–$O_{alkoxide}$ BCP has the largest electron density of all metal–ligand contacts in this work (ρ = 0.111 a.u.), a clearly negative H (−0.024 a.u.), |V|/G = 1.42 and ELF = 0.58, characteristic of a polar bond with substantial covalent character, whereas the Pb–O_{ester} (ρ = 0.049 a.u.; |V|/G = 1.16) and Pb···O=C (ρ = 0.017 a.u.; |V|/G = 0.90) contacts are intermediate and closed-shell, respectively.

Table 2. QTAIM descriptors (atomic units) at selected BCPs and Espinosa local interaction-energy estimates E_{BCP} = ½V (kcal mol^{-1}; relative indicator only). $O_{C=O}$, carbonyl oxygen (O50); O_{OH}/O_{alk}, hydroxyl/alkoxide oxygen (O38); O_{est}, ester ether oxygen (O13); O_w, water oxygen. Atom numbering follows that of the optimized structures.

Interaction	d (Å)	ρ	□²ρ	G	V	H	|V|/G	ELF	E(BCP)
Pristine copolymer segment									
O38–H39···N40	1.946	0.0360	0.1006	0.0283	–0.0314	–0.0031	1.11	0.137	–9.8
Cu, implicit water									
Cu–O(OH)	1.965	0.0758	0.5780	0.1449	–0.1453	–0.0004	1.00	0.067	–45.6
Cu–O(C=O)	1.995	0.0694	0.5266	0.1295	–0.1274	0.0021	0.98	0.063	–40.0
O38–H39···N40	1.871	0.0413	0.1097	0.0318	–0.0361	–0.0044	1.14	0.165	–11.3
Pb, implicit water									
Pb–O(alk)	2.055	0.1113	0.4645	0.0586	–0.0829	–0.0243	1.42	0.580	–26.0
Pb–O(est)	2.417	0.0490	0.1917	0.0250	–0.0290	–0.0040	1.16	0.270	–9.1
Pb···O(C=O)	2.959	0.0166	0.0566	0.0094	–0.0085	0.0010	0.90	0.074	–2.7
O38···H39–N40+	1.996	0.0264	0.1112	0.0258	–0.0237	0.0020	0.92	0.064	–7.4
Cu, explicit water									
Cu–O(C=O)	1.995	0.0672	0.5099	0.1245	–0.1216	0.0029	0.98	0.062	–38.2
Cu–O(w) (O55)	1.991	0.0725	0.5330	0.1335	–0.1337	–0.0002	1.00	0.068	–42.0
Cu–O(OH)	2.142	0.0506	0.3486	0.0810	–0.0749	0.0061	0.92	0.057	–23.5
O38–H39···O(w)52	1.577	0.0625	0.1909	0.0566	–0.0655	–0.0089	1.16	0.200	–20.6
O(w)55–H57···O(w)58	1.467	0.0789	0.1930	0.0692	–0.0901	–0.0209	1.30	0.266	–28.3
O(w)52–H54···O(w)55	1.833	0.0351	0.1213	0.0311	–0.0319	–0.0008	1.02	0.107	–10.0
Pb, explicit water									
Pb–O(alk)	2.163	0.0866	0.3476	0.0433	–0.0585	–0.0152	1.35	0.501	–18.4
Pb–O(w) (O58)	2.296	0.0615	0.2639	0.0328	–0.0389	–0.0061	1.18	0.325	–12.2
Pb–O(w) (O55)	2.317	0.0601	0.2475	0.0318	–0.0382	–0.0064	1.20	0.315	–12.0
Pb–O(C=O)	2.558	0.0323	0.1382	0.0201	–0.0197	0.0003	0.98	0.118	–6.2
O38···H39–O(w)52	1.460	0.0858	0.1819	0.0711	–0.0968	–0.0256	1.36	0.312	–30.4
O(w)55–H56···O(w)52	1.577	0.0629	0.1804	0.0547	–0.0644	–0.0096	1.18	0.214	–20.2
N40–H53···O(w)52	1.863	0.0336	0.1163	0.0295	–0.0300	–0.0005	1.02	0.104	–9.4

© 2026 Jusan Science Publisher LTD. All rights reserved.

This is an open access article distributed under the terms of the Creative Commons Attribution (CC BY 4.0) license.

In explicit water (Figures 5d and 5e), additional BCPs connect the metals to water oxygen atoms and link the water molecules to the polymer. For Cu, the three Cu–O BCPs (ρ = 0.051–0.073 a.u., |V|/G = 0.92–1.00, H ≈ 0) retain the electrostatic character found in implicit water, and the strongest new interactions are the water-mediated hydrogen bonds (ρ = 0.063 and 0.079 a.u., H < 0). For Pb, all Pb–O BCPs except the long carbonyl contact have negative H and |V|/G = 1.18–1.35, and the Pb–$O_{alkoxide}$ bond again has the largest ρ (0.087 a.u.). Summed over all metal–oxygen BCPs, the electron density is larger for Pb than for Cu in both solvation models (0.177 vs 0.145 a.u. in implicit water; 0.240 vs 0.190 a.u. in explicit water), reflecting the higher coordination number and covalency of Pb, whereas the Espinosa estimates, which are dominated by the large energy densities of the short Cu–O contacts, are larger in magnitude for Cu (ΣE_{BCP} = −85.6 and −103.6 kcal mol^{-1} for Cu vs −37.8 and −48.7 kcal mol^{-1} for Pb in implicit and explicit water, respectively). The descriptors therefore do not define a common affinity order: Cu forms shorter and more electrostatic contacts, whereas Pb forms longer but more covalent and more numerous contacts. Because none of these local quantities is a binding free energy, they cannot by themselves establish selectivity (Sections 3.5 and 3.6).

3.4 Electron Localization Function.

Figure 6 shows ELF maps for the two explicit-water complexes. ELF values close to 1 denote paired, localized electrons (covalent bonds and lone pairs), values around 0.5 correspond to electron-gas-like delocalization, and low values indicate regions between localization domains, typical of ionic or closed-shell contacts [33].

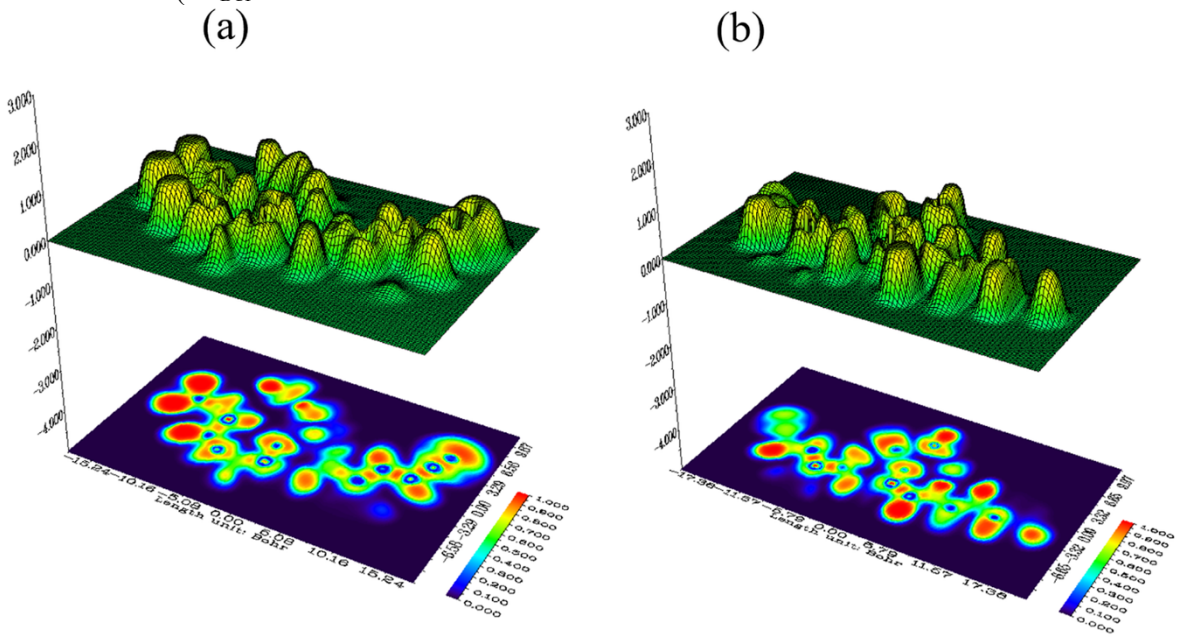

Figure 6. Electron localization function of (a) GMA/ACN/PEI copolymer segment with copper ion in the presence of explicit water molecules, and (b) GMA/ACN/PEI copolymer segment with lead ion in the presence of explicit water molecules.

In both maps, the high-ELF regions are associated with the covalent framework and the lone pairs of the oxygen and nitrogen atoms. For the Cu complex (Figure 6a), the Cu–O contact regions are electron-depleted: ELF at the three Cu–O BCPs is only 0.057–0.068 (Table 2), indicating that the oxygen lone pairs remain localized on the donors and that the Cu–O interactions are largely ionic, in agreement with the QTAIM classification. For the Pb complex (Figure 6b), ELF at the Pb–O BCPs is markedly higher (0.50 for Pb–$O_{alkoxide}$ and 0.32–0.33 for Pb–O_w), indicating a greater degree of electron sharing between Pb and its oxygen donors. ELF therefore confirms, independently of ρ and the energy densities, that Pb–O bonding is more covalent than Cu–O bonding in these models.

3.5 Integrated Interpretation and Comparison with Experiment.

Taken together, the geometric, RDG/NCI, QTAIM and ELF results give a consistent picture of two distinct binding modes rather than a single affinity ranking. (i) Cu binds to neutral oxygen donors (carbonyl, hydroxyl and water) through short (1.97–2.14 Å), predominantly electrostatic contacts with

© 2026 Jusan Science Publisher LTD. All rights reserved.
This is an open access article distributed under the terms of the Creative Commons Attribution (CC BY 4.0) license.

little electron sharing (H ≈ 0, |V|/G ≈ 1, ELF_{BCP} ≈ 0.06), and the hydroxyl group remains protonated. (ii) Pb binding is coupled to deprotonation of the β-hydroxyl group, the proton being accepted by the adjacent tertiary amine either directly (implicit water) or through a water bridge (explicit water). The resulting Pb–alkoxide bond is the most covalent metal–ligand interaction in this study (ρ = 0.087–0.111 a.u., H < 0, |V|/G = 1.35–1.42, ELF_{BCP} = 0.50–0.58), and it is complemented by ester, carbonyl and water oxygen donors in a hemidirected, higher-coordinate sphere. In both cases, the PEI amines act cooperatively with the hydroxyl group rather than as direct ligands, so that the amino-alcohol unit formed by epoxide ring opening is the key functional site of the adsorbent.

It should be emphasized that these descriptors do not indicate a general preference of the copolymer segment for Cu(II). On the contrary, the deprotonation-assisted, multidentate binding mode found for Pb provides a molecular rationale for the experimental observation that GMA/ACN/PEI adsorbents remove Pb(II) more efficiently than Cu(II): removal efficiencies of 85.6% vs 77.8% and Langmuir capacities of 15.25 vs 2.45 mg g^{-1} (≈ 0.074 vs 0.038 mmol g^{-1}) were reported [1]. Simple hard–soft acid–base arguments [37] would suggest a preference of Cu^{2+} for hard oxygen donors, but both ions are borderline acids, and the present results show that the protonation equilibrium of the amino-alcohol fragment, which HSAB arguments do not capture, can determine the binding mode. A definitive assignment of selectivity nevertheless requires the free-energy calculations outlined below.

3.6 Validation, Robustness, and Limitations of the Computational Model

Several checks support the robustness of the trends reported above. First, the computed metal–oxygen distances fall within the ranges typical of experimental structures: the Cu–O distances of 1.97–2.00 Å agree with the equatorial Cu(II)–O distances of about 1.96 Å in hydrated Cu(II) [38], and the Pb–O distances of 2.06–2.56 Å span the range between short Pb–O(alkoxide/hydroxide) bonds and the longer Pb–O(water) bonds of about 2.5 Å reported for hydrated Pb(II) [35], [38]. Second, all qualitative conclusions—exclusive oxygen coordination, the absence of metal–nitrogen bonds, retention of the hydroxyl proton for Cu, proton transfer for Pb and the larger covalency of the Pb–$O_{alkoxide}$ bond—are reproduced independently by the implicit and the cluster–continuum models, which differ substantially in their description of the first solvation shell. Third, the descriptors of the covalent framework remote from the binding site are virtually identical in all five systems (e.g. ρ = 0.238 a.u. at the C≡N BCP throughout), showing that the differences discussed above are localized at the binding site and are not numerical artefacts of the wavefunction analysis.

The model also has limitations that define the scope of the conclusions. (i) The LANL2DZ basis set lacks polarization functions on the light atoms and no dispersion correction was applied; this leads to systematically elongated multiple bonds (C=O = 1.247 Å and C≡N = 1.181 Å, compared with about 1.20–1.21 Å and 1.16 Å in experimental ester and nitrile structures) and may affect weak dispersion-bound contacts, although both metals are treated at the same level, so that relative structural trends are less affected. (ii) As noted in Section 3.1, UB3LYP places the unpaired electron of the Cu complexes largely on the amine fragment; whether this reflects genuine Cu(II)/amine redox chemistry or the delocalization error of the functional [36] should be tested with range-separated or higher-exact-exchange functionals (e.g. ωB97X-D or M06-2X) and larger basis sets (e.g. def2-TZVP with the corresponding ECPs). (iii) Each complex is represented by a single optimized conformer with one protonation and hydration pattern (three explicit water molecules), whereas the real adsorbent contains extended, cross-linked chains, pH-dependent amine protonation and metal ions with complete hydration shells.

(iv) Most importantly, binding energies and aqueous complexation free energies were not computed. Reliable values for divalent cations would require a thermodynamic cycle referenced to the fully hydrated ions (e.g. $[Cu(H_2O)_6]^{2+}$ and hydrated Pb^{2+}), counterpoise and standard-state corrections, conformational sampling and an explicit treatment of the released protons. Single-structure gas-phase or continuum binding energies would be dominated by the very large ion desolvation terms and could be misleading for selectivity. These calculations are beyond the scope of the present electronic-structure study and constitute the main direction of future work. Accordingly, the conclusions of this work are restricted to the binding modes and the nature of the metal–ligand interactions, and statements on selectivity are made only in comparison with the experimental data [1]

❖

4 Conclusion

© 2026 Jusan Science Publisher LTD. All rights reserved.
This is an open access article distributed under the terms of the Creative Commons Attribution (CC BY 4.0) license.

In this work, DFT calculations (UB3LYP/LANL2DZ with IEFPCM and a cluster–continuum model) combined with quantitative QTAIM, RDG/NCI and ELF analyses were used to characterize the interactions of a GMA/ACN/PEI copolymer segment with Cu and Pb. Both metals coordinate exclusively through oxygen donors—the ester carbonyl, the β-hydroxyl (or alkoxide) group formed by epoxide ring opening, the ester oxygen and water—whereas the PEI tertiary amines act as hydrogen-bond and proton acceptors rather than as direct ligands. Cu forms short Cu–O contacts (1.97–2.14 Å) of predominantly electrostatic character (ρ_{BCP} = 0.051–0.076 a.u., H ≈ 0, |V|/G ≈ 1, ELF_{BCP} ≈ 0.06), and the hydroxyl group remains protonated. Pb binding is accompanied by proton transfer from the hydroxyl group to the adjacent amine, directly or via a water bridge, producing a Pb–alkoxide bond (2.06–2.16 Å) with partial covalent character (ρ_{BCP} = 0.087–0.111 a.u., H < 0, |V|/G = 1.35–1.42, ELF_{BCP} = 0.50–0.58) within a hemidirected, up to four-coordinate sphere.

Explicit water molecules enter the coordination sphere of both metals, increase their coordination numbers and form extended hydrogen-bond networks; for Pb, they also act as a proton shuttle between the hydroxyl group and the amine. At the present level of theory, electron density is transferred from the amine fragment to Cu, giving the Cu complexes partial Cu(I)/aminium-radical character; this model sensitivity should be examined with other functionals.

The quantitative descriptors do not indicate an intrinsic preference of the copolymer segment for Cu(II). Instead, the deprotonation-assisted, multidentate binding of Pb(II) offers a molecular explanation for the higher experimental uptake of Pb(II) than Cu(II) by GMA/ACN/PEI adsorbents and identifies the amino-alcohol unit formed by epoxide ring opening as the key functional site for adsorbent design. Future work will address aqueous complexation free energies through thermodynamic cycles referenced to the hydrated ions, larger and more flexible polymer models with conformational sampling, pH-dependent protonation states, and benchmarking with larger basis sets and alternative functionals.

Funding

This research was funded by the Science Committee of the Ministry of Science and Higher Education of the Republic of Kazakhstan under the project "Multiscale modeling and experimental investigation of novel solvents for glycerol removal from biodiesel," grant AP27511369.

Data Availability Statement

The data supporting the findings of this study, including the Cartesian coordinates of the optimized structures, the complete QTAIM critical-point data, Gaussian output, wavefunction and Multiwfn files, are available from the corresponding author upon reasonable request.

Acknowledgements and AI Disclosure

The authors used ChatGPT (as disclosed in the submitted manuscript) only for language editing and rephrasing. They report that AI was not used to generate data, calculations, figures, analyses, or scientific conclusions. All scientific content and interpretations remain the responsibility of the authors.

Author Contributions

A.B. and N.B.: Conceptualization, methodology, literature review, and writing - original draft; A.A.: Conceptualization, methodology, data curation, visualization, and writing - review and editing; D.K.: Literature review, data curation, visualization, and writing - original draft; M.K.: Methodology, computational analysis, validation, visualization, supervision, writing - original draft, and writing - review and editing. J.L.: Contribution to be confirmed by the authors prior to publication. All authors should approve the final manuscript.

Conflict of Interest

The authors declare no conflict of interest.

Correspondence

Correspondence and requests for materials should be addressed to Mirat Karibayev (mirat.karibayev@nu.edu.kz).

© 2026 Jusan Science Publisher LTD. All rights reserved.
This is an open access article distributed under the terms of the Creative Commons Attribution (CC BY 4.0) license.

REFERENCES

[1] N. Bektenov, A. Baidullayeva, T. Chalov, T. Jumadilov, and K. Sadykov, "Modified adsorbents based on glycidyl methacrylate copolymers for the removal of copper and lead ions from wastewater," *Engineered Science*, vol. 31, Art. no. 1237, 2024. https://doi.org/10.30919/es1237

[2] N. Bektenov, K. Sadykov, A. Baidullayeva, N. Chinibayeva, T. Chalov, G. Koszhanova, and E. Kambarova, "Vermiculite Modified with Glycidyl Methacrylate, Acrylonitrile, and Phosphoric Acid for the Adsorption of Molybdenum and Rhenium Ions from Aqueous Solutions," *Processes*, vol. 13, no. 5, Art. no. 1584, 2025. https://doi.org/10.3390/pr13051584

[3] R. Tyagi and J. Jacob, "Highly porous, water-swellable, and reusable chelating polymeric gels for heavy metal ion removal from aqueous waste," *Journal of Applied Polymer Science*, vol. 138, no. 46, 2021. https://doi.org/10.1002/app.51353

[4] S. Chu, X. Feng, C. Liu, H. Wu, and X. Liu, "Advances in chelating resins for adsorption of heavy metal ions," *Industrial & Engineering Chemistry Research*, vol. 61, no. 31, pp. 11309–11328, 2022. https://doi.org/10.1021/acs.iecr.2c01353

[5] L. Chen, L. Lü, W. Shao, and F. Luo, "Kinetics and Equilibria of Cd(II) Adsorption onto a Chemically Modified Lawny Grass with H[BTMPP]," *Journal of Chemical & Engineering Data*, vol. 56, no. 4, pp. 1059–1068, 2011. https://doi.org/10.1021/je101037x

[6] A. Akhmetzhan, N. Myrzakhmetova, N. Amangeldi, Z. Kuanyshova, N. Akimbayeva, S. Dosmaganbetova, Z. Toktarbay, and S. N. Longinos, "A short review on the N,N-dimethylacrylamide-based hydrogels," *Gels*, vol. 7, no. 4, Art. no. 234, 2021. https://doi.org/10.3390/gels7040234

[7] A. Saeed, M. Iqbal, and M. W. Akhtar, "Removal and recovery of lead(II) from single and multimetal (Cd, Cu, Ni, Zn) solutions by crop milling waste (black gram husk)," *Journal of Hazardous Materials*, vol. 117, no. 1, pp. 65–73, 2004. https://doi.org/10.1016/j.jhazmat.2004.09.008

[8] J. K. Adjei, A. Ofori, H. K. Megbenu, T. Ahenguah, A. K. Boateng, G. A. Adjei, J. K. Bentum, and D. K. Essumang, "Health risk and source assessment of semi-volatile phenols, p-chloroaniline and plasticizers in plastic packaged (sachet) drinking water," *Science of the Total Environment*, vol. 797, Art. no. 149008, 2021. https://doi.org/10.1016/j.scitotenv.2021.149008

[9] M. O. A. El-Magied, M. M. Rezk, M. A. Youssef, E. M. Eldesouky, A. a. M. A. El-Hamid, W. M. Morse, W. S. Hafez, and E. A. Manaa, "Utilizing modified glycidyl methacrylate resins to remove chromium (VI) species from aqueous solutions," *Journal of Dispersion Science and Technology*, 1–10, 2025. https://doi.org/10.1080/01932691.2025.2502874

[10] B. Marković, G. Janjić, A. Onjia, T. Tadić, P. Stefanov, and A. Nastasović, "Experimental and quantum mechanical studies of efficient RE(VII)/MO(VI) separation by a magnetic Amino-Functionalized polymer," *Separations*, vol. 12, no. 8, Art. no. 206, 2025. https://doi.org/10.3390/separations12080206

[11] M. M. Bhuyan and J. Jeong, "Preparation of hydrogel by crosslinking and Multi-Dimensional applications," *Gels*, vol. 11, no. 11, Art. no. 896, 2025. https://doi.org/10.3390/gels11110896

[12] N. Xia, F. Gao, Z. Yu, S. Yu, and X. Yi, "Progress in the design and application of chemical and biological sensors based on atom transfer radical polymerization," *Biosensors*, vol. 15, no. 11, Art. no. 752, 2025. https://doi.org/10.3390/bios15110752

[13] A. Honciuc, A. Solonaru, and M. Honciuc, "Pickering Emulsion Polymerization Technology─Toward Nanostructured Materials for Applications in Metal Ion Extractions from Wastewaters," *ACS Applied Polymer Materials*, vol. 5, no. 10, pp. 8012–8022, 2023. https://doi.org/10.1021/acsapm.3c01267

[14] B. Sanay, R. Bozbay, S. Ciftbudak, Z. Ulker, S. Teke, Z. Akyol, E. P. Ozdemir, and N. Orakdogen, "Epoxy-Functional (Alkyl)methacrylate-Based Hybrids Reinforced with Layered Silicate Montmorillonite: From Mechanistic Study to Sustainable Wastewater Treatment," *Gels*, vol. 11, no. 10, Art. no. 803, 2025. https://doi.org/10.3390/gels11100803

[15] A. Chyzy, P. Gnatowski, E. Piłat, M. Sienkiewicz, K. Wozniak, M. Wojnicka, K. Brzezinski, and M. E. Plonska-Brzezinska, "Formation and characterization of Xylitol-Modified glycidyl Methacrylate-Co-Ethyl methacrylate matrices for controlled release of antimicrobial compounds," *Molecules*, vol. 30, no. 15, Art. no. 3083, 2025. https://doi.org/10.3390/molecules30153083

[16] Y. Hou, Z. Fu, J. Luo, X. Liu, H. Sun, and G. Li, "Selective separation of rhenium from oxygen-pressure leach solution of molybdenite concentrate using modified D201 resin: Experiments and theoretical calculations," *Journal of Molecular Liquids*, vol. 408, Art. no. 125371, 2024. https://doi.org/10.1016/j.molliq.2024.125371

[17] J. Zhang, Y. Chen, W. Zhao, and Y. Li, "Arsenic removal from aqueous solutions by diethylenetriamine-functionalized resin: isotherm, kinetics, selectivity and mechanism," *Royal Society Open Science*, vol. 5, no. 9, Art. no. 181013, 2018. https://doi.org/10.1098/rsos.181013

© 2026 Jusan Science Publisher LTD. All rights reserved.
This is an open access article distributed under the terms of the Creative Commons Attribution (CC BY 4.0) license.

[18] Y. Sailaukhanuly, A. Popova, T. Mansur, K. Bexeitova, S. Azat, K. Toshtay, A. Tovassarov, and A. Tasmagambetova, "Preliminary Study and Assessment of Drinking Water from Almaty, Kazakhstan," *Eurasian Chemico-Technological Journal*, vol. 24, no. 4, 2022. https://doi.org/10.18321/ectj1478

[19] H. K. Megbenu, Z. Tauanov, C. Daulbayev, S. G. Poulopoulos, and A. Baimenov, "Effective removal of methylene blue dye by a novel 4-vinylpyridine-co-methacrylic acid cryogel: kinetic, isotherm, and breakthrough studies," *Journal of Chemical Technology & Biotechnology*, vol. 97, no. 12, pp. 3375–3384, 2022. https://doi.org/10.1002/jctb.7197

[20] M. J. Frisch, G. W. Trucks, H. B. Schlegel, G. E. Scuseria, M. A. Robb, R. J. Cheeseman, *et al*., *Gaussian 16*, Revision C.01. Wallingford, CT, USA: Gaussian, Inc., 2016.

[21] A. D. Becke, "Density-functional thermochemistry. III. The role of exact exchange," *The Journal of Chemical Physics*, vol. 98, pp. 5648–5652, 1993. https://doi.org/10.1063/1.464913

[22] C. Lee, W. Yang, and R. G. Parr, "Development of the Colle–Salvetti correlation-energy formula into a functional of the electron density," *Physical Review B*, vol. 37, pp. 785–789, 1988. https://doi.org/10.1103/PhysRevB.37.785

[23] P. J. Hay and W. R. Wadt, "Ab initio effective core potentials for molecular calculations. Potentials for K to Au including the outermost core orbitals," *The Journal of Chemical Physics*, vol. 82, pp. 299–310, 1985. https://doi.org/10.1063/1.448975

[24] W. R. Wadt and P. J. Hay, "Ab initio effective core potentials for molecular calculations. Potentials for main group elements Na to Bi," *The Journal of Chemical Physics*, vol. 82, pp. 284–298, 1985. https://doi.org/10.1063/1.448800

[25] J. Tomasi, B. Mennucci, and R. Cammi, "Quantum mechanical continuum solvation models," *Chemical Reviews*, vol. 105, pp. 2999–3094, 2005. https://doi.org/10.1021/cr9904009

[26] R. Dennington, T. A. Keith, and J. M. Millam, *GaussView*, Version 6. Shawnee Mission, KS, USA: Semichem Inc., 2016.

[27] W. Humphrey, A. Dalke, and K. Schulten, "VMD: Visual molecular dynamics," *Journal of Molecular Graphics*, vol. 14, no. 1, pp. 33–38, 1996. https://doi.org/10.1016/0263-7855(96)00018-5

[28] T. Lu and F. Chen, "Multiwfn: A multifunctional wavefunction analyzer," *Journal of Computational Chemistry*, vol. 33, no. 5, pp. 580–592, 2012. https://doi.org/10.1002/jcc.22885

[29] E. R. Johnson, S. Keinan, P. Mori-Sánchez, J. Contreras-García, A. J. Cohen, and W. Yang, "Revealing noncovalent interactions," *Journal of the American Chemical Society*, vol. 132, pp. 6498–6506, 2010. https://doi.org/10.1021/ja100936w

[30] R. F. W. Bader, "A quantum theory of molecular structure and its applications," *Chemical Reviews*, vol. 91, pp. 893–928, 1991. https://doi.org/10.1021/cr00005a013

[31] E. Espinosa, E. Molins, and C. Lecomte, "Hydrogen bond strengths revealed by topological analyses of experimentally observed electron densities," *Chemical Physics Letters*, vol. 285, pp. 170–173, 1998. https://doi.org/10.1016/S0009-2614(98)00036-0

[32] E. Espinosa, I. Alkorta, J. Elguero, and E. Molins, "From weak to strong interactions: A comprehensive analysis of the topological and energetic properties of the electron density distribution involving X–H···F–Y systems," *The Journal of Chemical Physics*, vol. 117, pp. 5529–5542, 2002. https://doi.org/10.1063/1.1501133

[33] A. D. Becke and K. E. Edgecombe, "A simple measure of electron localization in atomic and molecular systems," *The Journal of Chemical Physics*, vol. 92, pp. 5397–5403, 1990. https://doi.org/10.1063/1.458517

[34] R. D. Shannon, "Revised effective ionic radii and systematic studies of interatomic distances in halides and chalcogenides," *Acta Crystallographica Section A*, vol. 32, pp. 751–767, 1976. https://doi.org/10.1107/S0567739476001551

[35] L. Shimoni-Livny, J. P. Glusker, and C. W. Bock, "Lone pair functionality in divalent lead compounds," *Inorganic Chemistry*, vol. 37, pp. 1853–1867, 1998. https://doi.org/10.1021/ic970909r

[36] A. J. Cohen, P. Mori-Sánchez, and W. Yang, "Insights into current limitations of density functional theory," *Science*, vol. 321, pp. 792–794, 2008. https://doi.org/10.1126/science.1158722

[37] R. G. Pearson, "Hard and soft acids and bases," *Journal of the American Chemical Society*, vol. 85, pp. 3533–3539, 1963. https://doi.org/10.1021/ja00905a001

[38] I. Persson, "Hydrated metal ions in aqueous solution: How regular are their structures?," *Pure and Applied Chemistry*, vol. 82, pp. 1901–1917, 2010. https://doi.org/10.1351/PAC-CON-09-10-22

© 2026 Jusan Science Publisher LTD. All rights reserved.
This is an open access article distributed under the terms of the Creative Commons Attribution (CC BY 4.0) license.